Recoverable and Programmable Collapse from Folding Pressurized Origami Cellular Solids

S. Li,[1,*] H. Fang,[2] and K. W. Wang[2]
[1]Department of Mechanical Engineering, Clemson University, Clemson, South Carolina 29634, USA
[2]Department of Mechanical Engineering, University of Michigan, Ann Arbor, Michigan 48109, USA
(Received 3 February 2016; revised manuscript received 8 June 2016; published 9 September 2016)

We report a unique collapse mechanism by exploiting the negative stiffness observed in the folding of an origami solid, which consists of pressurized cells made by stacking origami sheets. Such a collapse mechanism is recoverable, since it only involves rigid folding of the origami sheets and it is programmable by pressure control and the custom design of the crease pattern. The collapse mechanism features many attractive characteristics for applications such as energy absorption. The reported results also suggest a new branch of origami study focused on its nonlinear mechanics associated with folding.

DOI: 10.1103/PhysRevLett.117.114301

Collapsible structures and materials have played vital roles in modern engineering for personal safety and equipment protection purposes; they can sustain significant deformation without inducing a large reaction force and absorb a substantial amount of energy. A vast variety of collapsible systems have been developed and implemented [1–3], among which the cellular solids (such as honeycomb core, lattice, foam, and their relatives) are particularly promising. These microarchitectured systems are inherently light weight, and more importantly, their collapsing performance can be designed for a large range by tailoring the underlying cellular topology [4–6]. However, despite of the rich design variety, the collapse behavior of cellular solids, as well as many other collapsible systems, originates from the plastic deformation of their constituent materials; as a result, their collapses are not recoverable, and the associated energy absorbing performance cannot be controlled on demand.

We report a recoverable and programmable collapse mechanism via the *rigid folding* of a stacked origami cellular solid that consists of embedded and pressurized tubular channels. Rigid-foldable origami folds via bending along the crease lines without deforming the facets; therefore, they can be made out of relatively stiff materials for broader application appeal, including actuation and morphing [7–11], deployable structures [12–17], robotic linkage mechanisms [18–22], and mechanical metamaterials with programmable properties such as a negative Poisson's ratio and multistability [23–28].

The reported collapse mechanism originates from a unique phenomenon that has never been exploited in origami folding before: pressure-induced negative stiffness. Because of the nonlinear relationship between the folding kinematics and enclosed volume change, the stacked origami with constant internal pressure starts to exhibit negative stiffness when the external compressive force reaches a critical level. As a result, the stacked origami will collapse via rapid folding if the external force continues to increase until the self-locking or fully folded configuration is reached. Unlike many aforementioned collapsible systems, the collapse of origami involves only folding, so it is recoverable once the external force is released.

Furthermore, we show that the collapse of stacked origami is programmable: The magnitude of the critical force to induce collapse can be adjusted by pressure control, and the range of deformation (or folding) associated with the negative stiffness can be controlled via crease customization and strategic pressurization. Therefore, the recoverable and programmable collapse of origami features a combination of many desired characteristics that could enable unprecedented performance for energy absorption, particularly for low-frequency and large-force scenarios.

The following sections will start from an example of a stacked origami cellular solid based on the classic Miura-Ori crease and discuss the physical origin and experimental verifications of the recoverable collapse via rigid folding. Then we will discuss the strategies of programming such collapse behaviors based on a more generic single collinear crease and selective pressurization.

Pressure-induced stiffness and collapsing.—The backbone of the origami cellular solid is a set of rigid-foldable sheets that are stacked and connected along their crease lines [Fig. 1(a)]. The stacked origami has naturally embedded tubular channels, so when pressurized it will fold to the configuration with the maximum enclosed volume. This is essentially a process of increasing entropy due to inner energy reduction via volume expansion [29]. The pressurization also generates stiffness, because any folding deformations away from the maximum volume configuration would be resisted by pressure: The higher the pressure, the stiffer it becomes. Since the origamis of interest are rigid foldable, their quadrilateral facets can be

assumed rigid and crease lines are treated as perfect hinges with negligible torsional stiffness. The mechanical work done by the pressure is conservative, so the total inner energy (Π) of the system is a potential function of the gauge pressure (P) and enclosed volume of the tubular channel (V) so that $\Pi = P(V - V^0)$, where V^0 is an arbitrary reference volume where the potential energy is set to zero. If an applied external force deforms the stacked origami via folding, the reaction force generated by the internal pressure is calculated based on the virtual work principle:

$$F_X = -P\frac{dV}{dX} = -P\frac{dV}{d\theta}\left(\frac{dX}{d\theta}\right)^{-1}, \quad (1)$$

where dX is the origami deformation along the orientation of applied force and θ is a folding angle that characterizes the amount of folding. The pressure-induced tangent stiffness at different folding configurations would be the variation of reaction force with respect to infinitesimal deformation: $K_X = \partial F_X/\partial X$. For rigid-foldable origami, folding is a one-degree-of-freedom mechanism so that the correlation between the enclosed volume (dV), external deformation (dX), and folding ($d\theta$) is fully determined by the crease patterns. Therefore, we have a large freedom, via the crease pattern design, to program the pressure-induced reaction force and stiffness characteristics. For example, a stacked origami solid based on the classical Miura-Ori crease shows anisotropic stiffness at the maximum volume configuration, and we can program this anisotropy via tailoring the crease design parameters (Appendix Sec. 1 [30]).

If the external force induces large deformations or folding, the effective tangent stiffness varies significantly at different folding configurations. For some crease patterns, such a stiffness can reach zero at a critical configuration and then becomes negative if the origami is folded further [an experimental example based on the Miura-Ori crease is shown in Figs. 1(b) and 1(c) and Appendix Sec. II [30]]. For clarity, we will refer to the critical folding configuration corresponding to zero stiffness as the "collapsing" point. Such a change in the sign of the equivalent stiffness can lead to the desired collapse behavior, because, in the negative stiffness region, the stacked origami can sustain a large deformation via folding without increasing the reaction force. During the collapsing process, the pressurized fluid is pushed out of the stacked origami to maintain the required constant pressure. If this fluid flow is unidirectional, the stacked origami can absorb external energy from the applied force, so that the absorbed energy $\Delta E = -P\Delta V$, where ΔV is the enclosed volume reduction. The maximum possible energy absorption is equal to the area of the region below the force displacement curves.

A closer observation on the force-deformation relationships in Eq. (1) and the experiment results reveals many unique and attractive characteristics of the pressure-induced collapse. Unlike the aforementioned previous

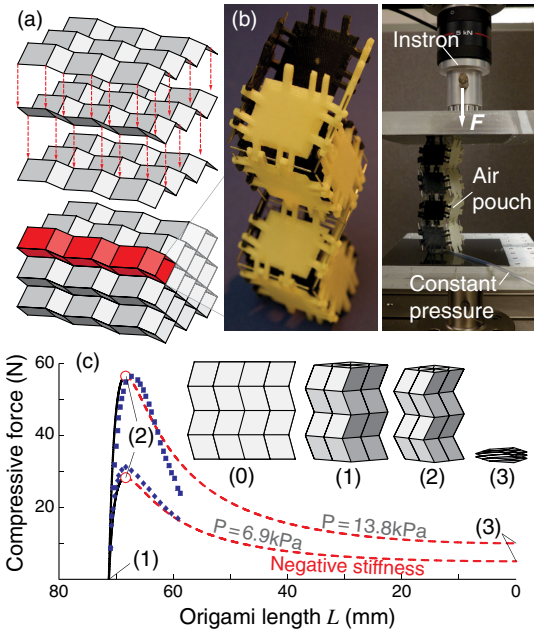

FIG. 1. Recoverable collapse from an example of a pressurized origami cellular solid. (a) Stacking origami sheets into a cellular solid with naturally embedded tubular channels. (b) A 3D printed channel prototype based on the Miura-Ori crease for a pressure-induced stiffness and collapse test. (c) The force-deformation relationships. Solid and dashed curves are analytical results; squares and diamonds are averaged experimental results. To-scale geometries of the Miura-Ori solids are illustrated at different important configurations: (0) flat sheet, (1) maximum volume configuration, (2) collapsing point, and (3) fully folded configuration.

studies, deformation or rigid folding of the staked origami does not involve any plastic material deformation; therefore, the origami will return to its maximum volume configuration once the external force is removed and the fluid is allowed to be pumped back into the origami, so that the collapsed structure is recoverable. Furthermore, the magnitude of the critical force corresponding to the collapsing point is linearly proportional to the internal pressure level, and deformations (or folding angles) associated with the negative stiffness region are solely functions of the crease design.

Programming the collapse behavior with single collinear vertices.—There are many different crease patterns that can enable the pressure-induced collapse, as long as their nonlinear folding kinematics shows a sign switch in dV/dX. Therefore, we have a large freedom to tailor the crease pattern and program the collapse behavior. Here we adopt a single collinear crease pattern for such a purpose, because it has a much richer crease design space compared to the classic Miura-Ori crease. It also has a *self-locking* mechanism so that we can prescribe the critical deformations corresponding to the start and ending of collapse.

The most fundamental element of the single collinear crease consists of one vertex and the four crease lines that

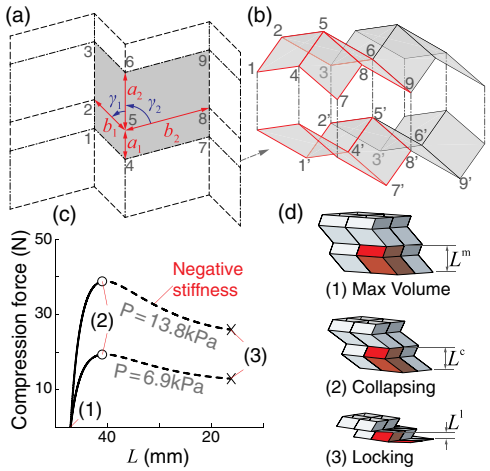

FIG. 2. Adopting single collinear vertices to program the collapse behavior. (a) A single collinear rigid-foldable origami sheet, where the elementary *vertex unit* is highlighted. (b) Identical origami sheets can be stacked into a cellular solid, where the equivalent vertices are labeled on both sheets to illustrate the stacking arrangement. (c) Force-displacement relationship based on an example design: $\gamma_1 = 60°$, $\gamma_2 = 75°$, $a_1 = 38$ mm, $a_2 = 57$ mm, $b_1 = 38$ mm, and $b_2 = 19$ mm. Notice that the negative stiffness region stops before the origami is fully folded to $L = 0$. (d) To-scale geometry of the origami cellular solids, with the unit cell being highlighted.

are connected to it [Fig. 2(a)]. The design of such vertex element is determined by six parameters that remain unchanged regardless of folding: They are the two collinear crease line lengths (a_1 and a_2), zigzag crease line lengths (b_1 and b_2), and two unique sector angles (γ_1 and γ_2). Without the loss of generality, we assume $0 < \gamma_1 \leq 90°$ and $\gamma_1 \leq \gamma_2 \leq 180° - \gamma_1$. Since γ_2 is assumed to be equal to or greater than γ_1 the facet 1-2-5-4 can touch facet 2-3-6-5 so that rigid folding is stopped before the vertex unit is fully folded into a flat state with $L = 0$. This mechanism is called *self-locking*, and it is an inherent property of single collinear vertices. A special case occurs when γ_1 equals γ_2, so that the vertex unit can be fully folded flat. The single collinear vertex therefore becomes *flat foldable*. A more special case occurs when $\gamma_1 = \gamma_2$, $a_1 = a_2$, and $b_1 = b_2$; the single collinear unit becomes the classic Miura-Ori crease (folding animations in Movie S1 [30]).

Identical single collinear origami sheets can be stacked and connected along their zigzag crease line to form a three-dimensional topology [Figs. 2(b) and 2(d)]. Its rigid folding is still a one-degree-of-freedom motion, and the constituent sheets reach the locking configuration simultaneously. Since the stacked origami is periodic, we will focus on the characteristics of an elementary *unit cell*, consisting of two vertex elements, as a representation of the whole system (Fig. 2; a tubular channel in the stacked origami is essentially a series of unit cells). Define nondimensional design parameters $\beta = b_2/b_1$ and $\kappa = \sin\gamma_2/\sin\gamma_1$, and the unit cell length (L) and its enclosed volume (V) are, respectively,

$$L = b_1 \sin\gamma_1 \frac{\cos\theta + \beta\sqrt{\kappa^2 - \sin^2\theta}}{\sqrt{1 - \sin^2\gamma_1 \sin^2\theta}}, \tag{2}$$

$$V = 2a_1 a_2 b_1 \sin^2\gamma_1 \sin\theta(\cos\theta + \beta\sqrt{\kappa^2 - \sin^2\theta}), \tag{3}$$

where the folding angle θ is defined as the dihedral angle between facet 1-2-5-4 and a reference x-y plane (Appendix Sec. 3 [30]). The folding angle θ^m corresponding to the maximum enclosed volume satisfies the following equation by solving $dV/d\theta = 0$:

$$\sin^6\theta - (1+\kappa^2)\sin^4\theta + \left[\frac{1-\kappa^4\beta^2}{4(1-\beta^2)} + \kappa^2\right]\sin^2\theta + \frac{\kappa^2(\kappa^2\beta^2 - 1)}{4(1-\beta^2)} = 0. \tag{4}$$

Therefore, θ^m is only a function of β and κ. If the origami is flat foldable ($\gamma_1 = \gamma_2$ and $\kappa = 1$), the enclosed volume equation (3) simplifies to $V = a_1 a_2 b_1 \sin^2\gamma_1(1+\beta)\sin 2\theta$. As a result, the maximum volume occurs at $\theta^m = 45°$ regardless of the crease line lengths.

By tailoring the single collinear crease design parameters, one can program the origami unit cell length at the maximum volume (L^m), collapsing (L^c), and locking (L^l) configurations. For a flat foldable vertex, γ_2 equals γ_1 ($\kappa = 1$), and its locking configurations is actually fully folded with $L^l = 0$. The reaction force equation (1) can be simplified into a nondimensional form:

$$\hat{F} = 2\frac{\cos 2\theta}{\sin\theta}\frac{\sin\gamma_1}{\cos^2\gamma_1}(1 - \sin^2\theta\sin^2\gamma_1)^{3/2}, \tag{5}$$

where the nondimensional force $\hat{F} = F/(Pa_1a_2)$. Therefore, the normalized collapse performance of a flat-foldable origami cell depends only on γ_1. Figure 3(a) illustrates some normalized force-deformation curves based on different γ_1 values; note that the two curves in the previous figure 1(c) with two different pressure levels are normalized to one curve in this figure. The critical folding angle at the occurrence of collapsing (θ^c) can be calculated by solving $dF/dL = 0$ so that

$$\sin^2\theta^c = \frac{1}{8}\left(1 + \frac{1 + \sqrt{\sin^4\gamma_1 + 10\sin^2\gamma_1 + 1}}{\sin^2\gamma_1}\right). \tag{6}$$

Define a nondimensional origami unit cell length $\hat{L} = L/(b_1 + b_2)$, and the relationships between $\hat{L}^m$, $\hat{L}^c$, $\hat{L}^l$, and γ_1 are shown in Fig. 3(b). Negative stiffness exits only when the sector angle $\gamma_1 > 45°$. When γ_1 equals 45°, collapsing occurs exactly at the fully folded configuration

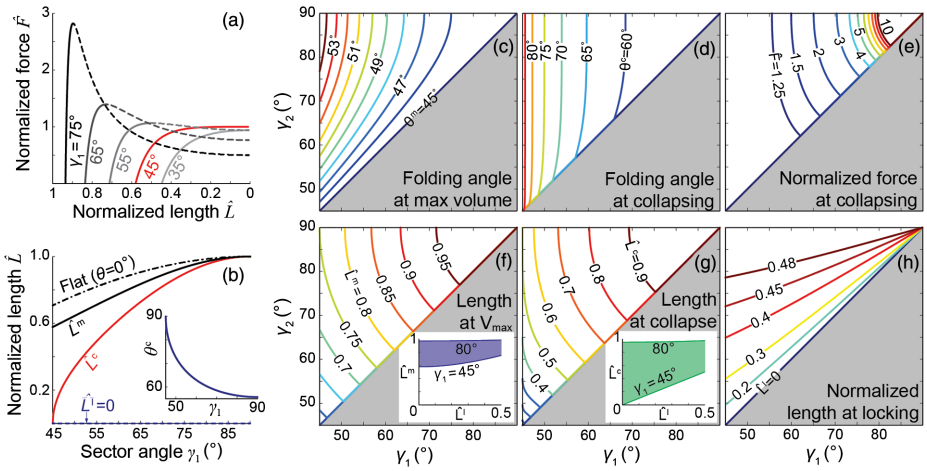

FIG. 3. The collapse performance based on different origami designs. (a) Normalized force-deformation curves of flat-foldable origami. (b) The lengths of a flat-foldable origami unit cell at different important configurations. The inset is the solution of Eq. (6). (c)–(h) Normalized collapse performance corresponding to generic single collinear creases, where the insets in (f) and (g) are achievable ranges of combinations of $\hat{L}^m$, $\hat{L}^c$, and $\hat{L}^l$. $\beta = 1$ in these figures, and figures with $\beta = 2$ and 0.5 are in Appendix Sec. V [30].

($\hat{L}^b = \hat{L}^l = 0$); as γ_1 increases from 45° to 90°, the collapsing point moves monotonically from the fully folded to the maximum volume configuration.

For generic single collinear vertices, the normalized collapse performance depends not only on sector angle γ_1 but also on γ_2 and the length ratio between the two zigzag crease lines (β). Figures 3(c)–3(f) and Supplemental Figs. S4 and S5 [30] illustrate the relationships between the collapse performance and these three crease designs variables. Negative stiffness exists only when sector angle $\gamma_1 \geq 45°$, and a closer examination of the results shown in Figs. 3(f)–3(h) reveals a large range of achievable combinations of $\hat{L}^m$, $\hat{L}^c$, and $\hat{L}^l$ (Appendix Sec. IV [30]). Therefore, by tailoring the three crease variables (γ_1, γ_2, and β), one has a large design space to program the desired deformations at collapsing and locking (restabilization).

Stacking different origami sheets for integrated performance.—Based on the correlations between the collapse performance and crease designs, one can assemble different origami sheets together into a foldable cellular solid featuring a fully programmable collapse in terms of both the critical force and deformations. For example, if the stacked origami consists of two different sheets (designated as sheets A and B), there can be three different unit cells depending on their arrangements (Fig. 4; see Appendix Sec. VI [30] for design constraints from stacking different sheets). The first type of cell is formed by stacking two sheets A, which is designated as an AA cell, and similarly there are AB and BB types of cells. This concept is illustrated and tested on a 3D printed tricell prototype [Fig. 4(b)]. Despite their unique geometries, all these cells reach locking simultaneously at a common locking length ($\hat{L}^l$). However, they have different values of $\hat{F}$ and $\hat{L}^c$ at collapsing, as well as $\hat{L}^m$ at the maximum volume [Figs. 4(c) and 4(d)]. Therefore, by selectively pressuring

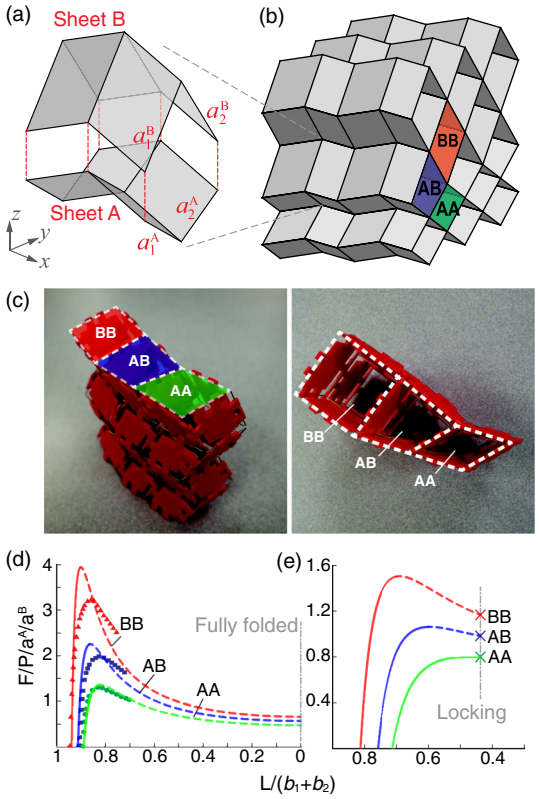

FIG. 4. Integrating different cells into a solid. (a) Two different sheets that meet specific geometric constraints can be stacked seamlessly together and form a foldable solid with three types of cells (b). (c) A 3D printed tricell prototype for concept testing, in this design: $\gamma_1^A = \gamma_1^B = 70°$, $\beta = 1$, and $a^B = 1.35a^A$. (d) Normalized collapse performance of the prototype design. The solid points are the corresponding averaged experimental results. (e) Normalized collapse performances from a generic single collinear design: $\gamma_1^A = 45°$, $\gamma_1^B = 70°$, $\beta = 1$, and $a^B = 1.25a^A$.

different types of cells at a desired level, one can control the collapse performance on demand.

In a broader scope, the analytical and experimental investigation of the programmable collapse from origami folding laid down the foundation for applying the pressurized origami solid for recoverable energy absorbers. Since the physical principles related to the underlying pressure-induced stiffness is primarily geometrical, the programmable collapse can be achieved with vastly different crease design length scales. The negative stiffness may also enhance the performance of the aforementioned applications of rigid origami folding such as rapid morphing and actuation [31], as well as enabling other high-performance dynamic applications that have not been attempted on origami systems, such as vibration isolation and damping at an extremely low frequency [32,33]. Finally, collapse and negative stiffness belong to the topic of nonlinear mechanics that is related to a large amplitude deformation (folding); the results of this Letter suggest potential richness in this topic, which can be developed into another branch of origami study.

This research is supported by the University of Michigan Mechanical Engineering Collegiate Professorship.

*To whom correspondence should be addressed.
suyil@clemson.edu

[1] A. A. A. Alghamdi, Thin-Walled Struct. **39**, 189 (2001).
[2] G. Lu and T. Yu, *Energy Absorption of Structures and Materials*, 1st ed. (Woodhead, Boca Raton, FL, 2003).
[3] P. Qiao, M. Yang, and F. Bobaru, J. Aerosp. Eng. **21**, 235 (2008).
[4] S. K. Maiti, L. J. Gibson, and M. F. Ashby, Acta Metall. **32**, 1963 (1984).
[5] S. M. Pingle, N. A. Fleck, V. S. Deshpande, and H. N. G. Wadley, Proc. R. Soc. A **467**, 985 (2011).
[6] A. G. Evans, J. W. Hutchinson, N. A. Fleck, M. F. Ashby, and H. N. G. Wadley, Prog. Mater. Sci. **46**, 309 (2001).
[7] R. V. Martinez, C. R. Fish, X. Chen, and G. M. Whitesides, Adv. Funct. Mater. **22**, 1376 (2012).
[8] L. Bowen, K. Springsteen, H. Feldstein, M. Frecker, T. W. Simpson, and P. von Lockette, J. Mech. Robot. **7**, 011010 (2015).
[9] J. T. B. Overvelde, T. A. de Jong, Y. Shevchenko, S. A. Becerra, G. M. Whitesides, J. C. Weaver, C. Hoberman, and K. Bertoldi, Nat. Commun. **7**, 10929 (2016).
[10] S. Li and K. W. Wang, Smart Mater. Struct. **24**, 105031 (2015).
[11] S. Li and K. W. Wang, J. R. Soc. Interface **12**, 20150639 (2015).
[12] T. Tachi, in *Origami 5 Proceedings of the Fifth International Meeting on Origami Science Mathematics Education*, edited by P. Wang-Iverson, R. J. Lang, and M. Yim, 1st ed. (A K Peters/CRC Press, Boca Raton, FL, 2011), pp. 253–264.
[13] J. M. Gattas and Z. You, Engineering structures **94**, 149 (2015).
[14] Y. Chen, R. Peng, and Z. You, Science **349**, 396 (2015).
[15] A. P. Thrall and C. P. Quaglia, Engineering structures **59**, 686 (2014).
[16] S. A. Zirbel, R. J. Lang, M. W. Thomson, D. A. Sigel, P. E. Walkemeyer, B. P. Trease, S. P. Magleby, and L. L. Howell, Journal of mechanical design **135**, 111005 (2013).
[17] Z. Y. Wei, Z. V. Guo, L. Dudte, H. Y. Liang, and L. Mahadevan, Phys. Rev. Lett. **110**, 215501 (2013).
[18] S. Felton, M. Tolley, E. D. Demaine, D. Rus, and R. Wood, Science **345**, 644 (2014).
[19] J. M. Gattas, W. Wu, and Z. You, Journal of mechanical design **135**, 111011 (2013).
[20] E. D. Demaine and J. O'Rourke, *Geometric Folding Algorithms: Linkages, Origami, Polyhedra*, 1st ed. (Cambridge University Press, Cambridge, England, 2007).
[21] D. Dureisseix, International Journal of space structures **27**, 1 (2012).
[22] D. Y. Lee, J. S. Kim, S. R. Kim, J. S. Koh, and K. J. Cho, in *Proceedings of the ASME International Design Engineering Technical Conference on Computing Information and Engineering* (ASME, Portland, OR, 2013).
[23] C. Lv, D. Krishnaraju, G. Konjevod, H. Yu, and H. Jiang, Sci. Rep. **4**, 5979 (2014).
[24] H. Yasuda and J. Yang, Phys. Rev. Lett. **114**, 185502 (2015).
[25] S. Waitukaitis, R. Menaut, Bryan Gin-ge Chen, and M. van Hecke, Phys. Rev. Lett. **114**, 055503 (2015).
[26] M. Schenk and S. D. Guest, Proc. Natl. Acad. Sci. U.S.A. **110**, 3276 (2013).
[27] M. Eidini and G. H. Paulino, Sci. Adv. **1**, e1500224 (2015).
[28] E. T. Filipov, T. Tachi, and G. H. Paulino, Proc. Natl. Acad. Sci. U.S.A. **112**, 12321 (2015).
[29] B. Gramüller, J. Boblenz, and C. Hühne, Smart Mater. Struct. **24**, 125027 (2014).
[30] See Supplemental Material at http://link.aps.org/supplemental/10.1103/PhysRevLett.117.114301 for additional information on stacked origami design, experiment materials and methods, and analysis results.
[31] N. Hu and R. Burgueño, Smart Mater. Struct. **24**, 063001 (2015).
[32] Y. C. Wang and R. S. Lakes, Philos. Mag. **84**, 3785 (2004).
[33] D. R. Johnson, M. Thota, F. Semperlotti, and K. W. Wang, Smart Mater. Struct. **22**, 115027 (2013).